Technical Note

Use of a Wearable Mobile Laser System in Seamless Indoor 3D Mapping of a Complex Historical Site

**Andrea di Filippo [1], Luis Javier Sánchez-Aparicio [2] , Salvatore Barba [1] ,
José Antonio Martín-Jiménez [2] , Rocío Mora [2] and Diego González Aguilera [2,*]**

[1] Department of Civil Engineering, University of Salerno, Via Giovanni Paolo II, 132, 84084 Fisciano (SA),
Italy; andrew89.adf@gmail.com (A.d.F.), sbarba@unisa.it (S.B.)

[2] Department of Land and Cartographic Engineering. University of Salamanca,
Higher Polytechnic School of Avila, Calle de los Hornos Caleros, 50, 05003 Avila, Spain;
luisj@usal.es (L.J.S.-A.); joseabula@usal.es (J.A.M.-J.); rociomora@usal.es (R.M.)

* Correspondence: daguilera@usal.es

check for
updates

Abstract: This paper presents an efficient solution, based on a wearable mobile laser system (WMLS), for the digitalization and modelling of a complex cultural heritage building. A procedural pipeline is formalized for the data acquisition, processing and generation of cartographic products over a XV century palace located in Segovia, Spain. The complexity, represented by an intricate interior space and by the presence of important structural problems, prevents the use of standard protocols such as those based on terrestrial photogrammetry or terrestrial laser scanning, making the WMLS the most suitable and powerful solution for the design of restoration actions. The results obtained corroborate with the robustness and accuracy of the digitalization strategy, allowing for the generation of 3D models and 2D cartographic products with the required level of quality and time needed to digitalize the area by a terrestrial laser scanner.

Keywords: cultural heritage; restoration; indoor mapping; laser scanning; wearable mobile laser system; 3D digitalization; SLAM

1. Introduction

The guidelines for the conservation and enhancement of cultural heritage, codified in the Athens Charter and repeatedly reiterated by subsequent documents up to the most recent Krakow Charter [1], underline the importance of multidisciplinary and scientific approaches for the management of interventions in cultural heritage sites [2].

Currently, the use of new technologies for the data acquisition in the architectural field has reached widespread diffusion, mainly due to the ability to digitalize artifacts with great precision and to the possibility of generating informative models useful for the analysis, simulation, and interpretation phases [3]. The most popular techniques, which have now become a reference standard, are modern photogrammetry [4] and laser scanning [5]. Photogrammetry acquires two-dimensional images that require mathematical processing to derive 3D information. Through precise formulations based on projective or perspective geometry [6], it transforms the data extracted from the images into three-dimensional metric coordinates and colors [7]. For its part, laser scanning is able to directly obtain the 3D point spatial position [8,9] with high accuracy and without lighting conditions, especially over homogeneous surfaces where photogrammetry cannot provide reliable results.

The main products obtained from both 3D point clouds and 2D orthoimages techniques have been used for the virtual reconstruction of cultural heritage sites [10], the analysis of rock-art

paintings [11,12], the creation of accurate numerical simulations [13], or even the analysis of pathological processes [14,15], among others.

Besides the wide range of advantages that these solutions can offer, the digitalization of large and complex areas, especially indoor scenarios, generally entails the use of a large amount of images (in the case of photogrammetry) or scan stations (in the case of the laser scanner), deriving in a time consuming fieldwork and thus in an important error propagation [16,17]. Hybrid solutions, such as mobile mapping systems (MMSs), have emerged with great capabilities and possibilities in the last few years, allowing the management of different sensors and the possibility to operate in complex outdoor and indoor scenarios [18–21], minimizing error propagation.

Since their early development in the late 1980s, MMSs have been progressively improved in order to provide increasingly more precise and denser data, acquired in a shorter amount of time [22]. Besides the progresses in optical sensors, one of the key advances in MMS is related to spatial referencing technology. While the very early applications were restricted to environments where the sensor positions were computed using ground control, advantages in satellite and inertial technology make spatial referencing possible in previously unknown and undiscovered places [23,24]. Furthermore, the miniaturization and cost reduction of components have played a fundamental role in the spread of MMS, allowing for more flexible, portable, and low-cost systems [22]. This attribute, within the capacity of generating 3D point clouds by means of a spatial referencing in previously unknown environments, has allowed the application of this technology in Unmanned Aerial Vehicles (UAV) [23,25,26], Unmanned Ground Vehicles (UGV) [27–29], or equipped in backs (e.g., the Leica Pegasus back-pack, the Heron MS-2 back-pack or the Kaarta Stencil) [22,24,30]. Meanwhile, the use of the two first platforms could reduce the problems associated with travelling speed during the data acquisition, as well as improving the time efficiency during the survey. Moreover, their application in indoor and narrow spaces (common in Cultural Heritage) could entail some problems. These limitations place the wearable mobile laser systems (WMLS) as a potential solution for mapping indoor environments, as it is possible to obtain a 3D point cloud of the environment with a centimeter's accuracy [22,24,30]. However, this accuracy could be strongly affected by the characteristics of the trajectory, such as the travelling speed or the path followed [22,31].

Under these assumptions, this paper evaluates the suitability of a wearable mobile laser system for the digitalization of a complex indoor environment belonging to a cultural heritage building, as well as for the generation of cartographic products required for its conservation and restoration. This wearable system combines laser scanning technology and an inertial measurement unit (IMU) in portable equipment that can be handled by an operator while walking through the cultural heritage site. This sensor acquires point clouds on the move, thanks to the Simultaneous Localization and Mapping algorithms (SLAM) [32,33], without needing the support of a global navigation satellite system (GNSS). During this evaluation, we took into account the different parameters that could influence the final quality of the 3D point cloud. These parameters are: (i) the identification of critical areas; (ii) the prevision for closing loops; (iii) the traveling speed; (iv) the time spent to obtain the 3D point cloud; and (v) the density of the point cloud.

2. Materials and Methods

2.1. Equipment

The WMLS tested in the case study was the ZEB-REVO, commercialized by GeoSLAM (Figure 1) [34], which consisted of a 2D time-of-flight laser scanner (Hokuyo UTM-30LX-F from Hokuyo Automatic Co., Osaka, Japan) rigidly coupled to an IMU mounted on a rotary engine. The motion of the scanning head on the motor drive was stored in a processing unit located in a small backpack and provided the third dimension to generate 3D information. This computer was equipped with batteries that fed the hand-held laser scanner through a special connection cable. A 3D SLAM algorithm was used to combine the 2D laser scan data with the IMU data, in order to return accurate

3D point clouds, following the full SLAM approach implemented in the robotic operative system (ROS) library [35]. With a 360° vertical field of view and 30 m of range in ideal indoor conditions (which was reduced to 15–20 m in real working circumstances), the operator moved through the indoor environment capturing more than 43,000 points per second. Regarding accuracy, the manufacturer declared that its value is 1–3 cm in relative terms and 1–30 cm in absolute positioning for a 10-min scan, with the closing of a single loop [34]. Table 1 shows further technical specifications.

Figure 1. Main components of the wearable mobile laser systems (WMLS) used for data acquisition.

Table 1. Technical specification of the Geo Simultaneous Localization and Mapping (SLAM) ZEB-REVO device.

Parameter	Value	Parameter	Value
Total device dimension (mm)	220 × 180 × 470	Laser measuring principle	Time of flight
Scanner dimension (mm)	86 × 112 × 287	Scanner resolution	0.625° H × 1.8° V
Total device weight (kg)	4.10	Wavelength (nm)	905
Scanner weight (kg)	1.00	Orientation system	MEMS IMU
Head rotation speed (Hz)	0.5	Camera	GoPro
Operating time (h)	4	Scan rate	100 lines/s 43,200 points/s
Field of view	270° (H) × 360° (V)	Points per scan line	432 (0.325° int)

2.2. Methodology

The formalization of a schematic procedural pipeline for data acquisition and management represents a fundamental step to test the effective possibility of using WMLS for tracking complex indoor environments.

In this regard, it is possible to identify a succession of methodological phases that characterize an inspection with this approach: (i) the survey design (planning of the path); (ii) the data acquisition (protocol and basic rules); (iii) the post-processing (SLAM algorithm to compute the sensor trajectory and map the environment); and (iv) the cartographic product generation (three-dimensional and two-dimensional digital models). Figure 2 outlines the main steps of the applied methodology.
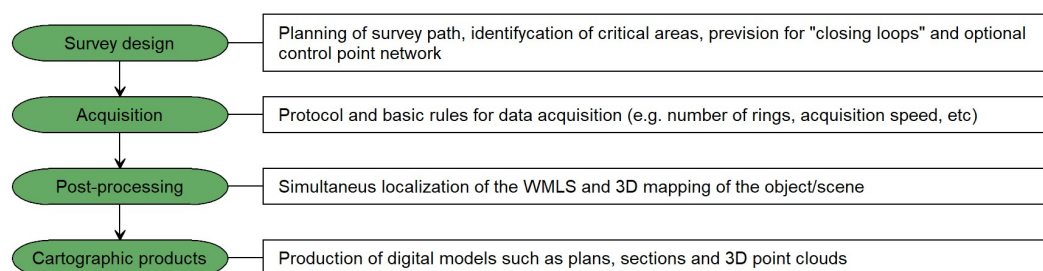
Figure 2. Methodological phases of the procedural pipeline for surveys with a WMLS.

2.2.1. Survey Design

Before conducting data acquisition, the user should plan the proposed survey path in order to identify potential problem areas, such as doorway transitions, stairwells, open spaces, and smooth walled passageways, generally with poor geometrical features. It should be noted that features are significant if the ratio of their size and their range is approximately 1:10 (e.g., a feature must be textgreater0.5 m in size for a distance of 5 m). In addition, if there are not sufficient features along the direction of travel, the SLAM algorithm cannot correctly determine forward motion. In these cases, the user can proceed in the following ways:

- Improve the background with additional references (e.g., boxes in a corridor or a parked vehicle in an open field);
- ensure that those limited features are scanned repeatedly as you move through the scene by pointing the WMLS in their direction. As a result, more measurement points will define the element, assuring its use as reference during the post-processing;
- avoid acquiring moving objects (e.g., passing pedestrians or vehicles) since the SLAM algorithm may support on them as static features.

The planning should also consider "closing loops" wherever possible. The approach used to transform the raw scan data into a point cloud uses a method analogous to the close traverse technique applied for surveys [36], in that a previously known position is used to determine its current location. The re-surveying of a known area allows the spreading of the compounded error around the loop and the improvement of the accuracy of the resulting point cloud. As a minimum, it is mandatory that the operator starts and ends the survey in the same position to ensure at least one loop closure (Figure 3).

In general, it is better to do circular loops rather than "there and back" loops where the path simply doubles back on itself [31]. This applies to horizontal and vertical rings—i.e., if possible enter and exit through different doors and move between floors via distinct stairwells. It is important to scan the closed loop regions carefully to ensure that the key features are scanned from a similar perspective. It may be necessary to turn around to return to a region from another direction. This is a crucial feature in poor environments.

Figure 3. Example of a survey design with the WMLS. The compensation of the accumulated error is possible thanks to the closure of the path following different track and acquiring the internal cloister area from different points of the route.

2.2.2. Acquisition

The process of scanning using WMLS is an important step since the collected data will inevitably influence the level of quality of the cartographic products. For these reasons, it is useful to define the following operative rules:

- Inspect the site of interest in advance in order to identify critical areas not detected during planning and remove any obstacles along the way;
- make easily accessible all the connections between different rooms and floors, such as doorways or stairs, so as to ensure safe passage of the operator and avoid moving objects during the scanning;
- walk slowly in order to have a good coverage and a high-resolution data. If the forward movement is too fast there may not be enough repeated features for the SLAM algorithm to transform the raw laser data into a point cloud;
- pay attention to the transition areas and tight curves that must be travelled slowly, guaranteeing a period when the scanner can display features on both sides. The same care is necessary when we change from a closed space (feature rich) to an open environment (feature poor);
- split large surveys into more than one scan mission. This is to avoid big file sizes as well as to reduce any drift effect and thus error propagation that might be created in the SLAM data. It is recommended that each scan mission is limited to 30 min [34].

2.2.3. Post-Processing: The Generation of the 3D Point Cloud

The post-processing approach adopted for the case study was the Simultaneous Localization and Mapping (SLAM) algorithm, which addressed the problem of positioning a mobile system in an unknown environment and provided its 3D mapping. Access to SLAM was justified in two ways: (i) placing the system within a space or environment (pose estimation or trajectory computation); (ii) 3D modelling of the environment (mapping or reconstruction).

A large variety of SLAM solutions are available; they can be classified either as filtering or smoothing [32]. Filtering approaches model the problem as an online state estimation, where the state of the system consists in the current instrument position and the map. The estimation is augmented and refined by incorporating new measurements as they become available. To highlight their incremental nature, filtering approaches are usually referred as online SLAM methods [37]. Conversely, smoothing approaches estimate the full trajectory of the instrument from the full set of measurements. They address the so-called full SLAM problem and typically rely on least-square error minimization techniques.

GeoSLAM algorithm is able to perform both an open-loop incremental solution for online SLAM and a closed-loop global registration for full SLAM (as in the case study). However, it is appropriate to introduce the general characteristics of the algorithm in order to understand its performance. For GeoSLAM formulation, the trajectory can describe the position of the sensor during data acquisition and can project raw laser measurements (2D laser profiles or segments) into a registered 3D point cloud when necessary. Data processing is an incremental (the segments are registered one-by-one) and iterative procedure following a framework similar to the iterative closest point (ICP) algorithm:

- The first step identified corresponding surface patches from the laser point cloud. The patches were determined by spatially decomposing the scene into a multiresolution voxel grid, controlled by the "voxel density" parameter; increasing it caused the algorithm to use smaller voxels. Clusters of laser points that were both spatially and temporally proximal were identified and used to compute surface properties based on the centralized second-order matrix of the point coordinates [33]. The surface normal was obtained from the eigenvector corresponding to the minimum eigenvalue of the second-order matrix. The surface planarity, computed from the ratio of the eigenvalues, was used to discard elements that were not approximately planar. These properties were used to establish a first registration of the segments. During this stage, the

following constrains were applied: (i) a filter for retaining only reciprocal correspondences and (ii) several boundary conditions that ensured continuity with the previous segment [33].

- In the second step, the estimated trajectory between two proximal surfaces was refined, minimizing the errors between matching surfaces and deviations from the measured IMU accelerations and rotational velocities. During this process, the following elements were considered into a cost-function (function to be minimized): (i) surface element match errors, (ii) IMU measurement deviations, and (iii) initial condition constraints. It is worth mentioning that the consideration of the IMU measurements ensured the estimated trajectory was smooth. The above terms of the cost-function were non-linear with respect to the rotational correction. Taking this into consideration, the algorithm used a linearization of the system by means of the Taylor expansion.

On the first iteration, the previously unprocessed trajectory segment was initialized by integrating the accelerometer and gyro measurements from the IMU. Since the processing window was advanced by a fraction of its length, the first section of the trajectory segment was already estimated from the previous time step; thus, the IMU data were only required to propagate the trajectory for the remainder of the window. As new data were acquired, the algorithm proceeded by processing a segment of the trajectory whose extremes were represented by positions occupied by the system in two well-defined moments. Next, it advanced the window by a fraction of its length from the previous time step. The dimension of segments was defined by the "window size" parameter. The number of iterations was controlled by the "convergence threshold" parameter; increasing it raised the maximum number of iterations for each processing step and reduced the convergence threshold during the online registration phase.

Considering that the previous process was an incremental procedure (also called open-loop solution) in which each segment was registered with respect to the previous segment, an error accumulation could be produced. In order to minimize the error accumulation, and considering that the data acquisition followed a close-loop path (Figure 3), the GeoSLAM algorithm applied a global registration procedure in which the close-loop restriction was taken into account. During this stage, the algorithm operated along the entire trajectory with one large window, instead of considering the trajectory in small segments (open-loop solution). Eventually, it was possible to give priority to flat surfaces in the search for feature correspondence. Moreover, it is worth mentioning that the laser scanner used by the tested WMLS was a line scanner (Figure 1) (Table 1). This laser was complemented with a rotational engine that allowed us to obtain a 2D profile in each period of time (segment of the scene). All of this was carried out by an operator. The movement of the operator along the scene guaranteed the acquisition of successive segments characterized by a certain overlap that the SLAM algorithm registered, allowing for the creation of the 3D point cloud.

2.2.4. Cartographic Products Generation

The generation of plants and sections required a vectorization of the 3D point cloud obtained from the fusion of the different paths. Thus, the following approach was carried out: (i) the extraction of sections from the 3D point cloud and (ii) the vectorization of the sections.

Regarding vectorization, the most efficient solutions are those that allow semi-automatic feature extraction from point clouds. The least-cost-path algorithms are particularly interesting [38] for our case study, since the automatic solutions are not able to recognize (and possibly not represent) the different objects in the scene and are influenced by the characteristic noise of the point clouds returned with a SLAM approach. Conceptually, a least-cost-path algorithm can be divided into two steps. In the first step, data points are linked with their nearest neighbors using a spherical search radius slightly larger than the point cloud resolution to produce a neighborhood network. A cost function, which represent the effort of moving along points in this network (hereafter referred to as "edges") is estimated. The second step derives the least-cost path between user-defined network points, providing

the estimated trace. Once a trace has been estimated, manual adjustments can be easily applied by adding intermediate waypoints and recalculating the relevant least-cost paths.

3. Results

3.1. Case Study: An XV Century Palace

With the aim of evaluating the potentialities and limitations of the WMLS technology, we selected a gothic palace in ruins, located in the urban center of Segovia (Castile and León, Spain), as a case study (Figure 4). The palace was erected in the 15th century as a consequence of the economic expansion experimented by the city, following the precepts of the civil plateresque architecture [39]. Its fronts are made of sandstone masonry and brick masonry. They stand out for their horizontality, showing a ratio height/width of 1/2. With respect to the inner composition, the construction shows the characteristic appearance of the palaces erected during this epoch, with two annular traces in the two first plans and an inner cloister in the center of the construction [39]. These elements are integrated on five levels: (i) basement; (ii) ground floor; (iii) mezzanine; (iv) first floor and; (v) gallery (maybe added during the XIX century), filling an area of about 3000 m^2 and holding more than 50 rooms. The internal courtyard is characterized by a front porch that transfers part of its weight to the masonry and partly to stone columns with granite base (Figure 5).

The construction is mainly made up of sandstone coming from the local quarries. In the lower part (foundations and basement) a masonry in stones connected with mortar prevails, to which a brick masonry and a half-timbered work are replaced, proceeding upwards (Figure 5).

Recent restoration measures have added structural elements in reinforced concrete, such as beams and pillars in order to avoid the collapse of the structure.
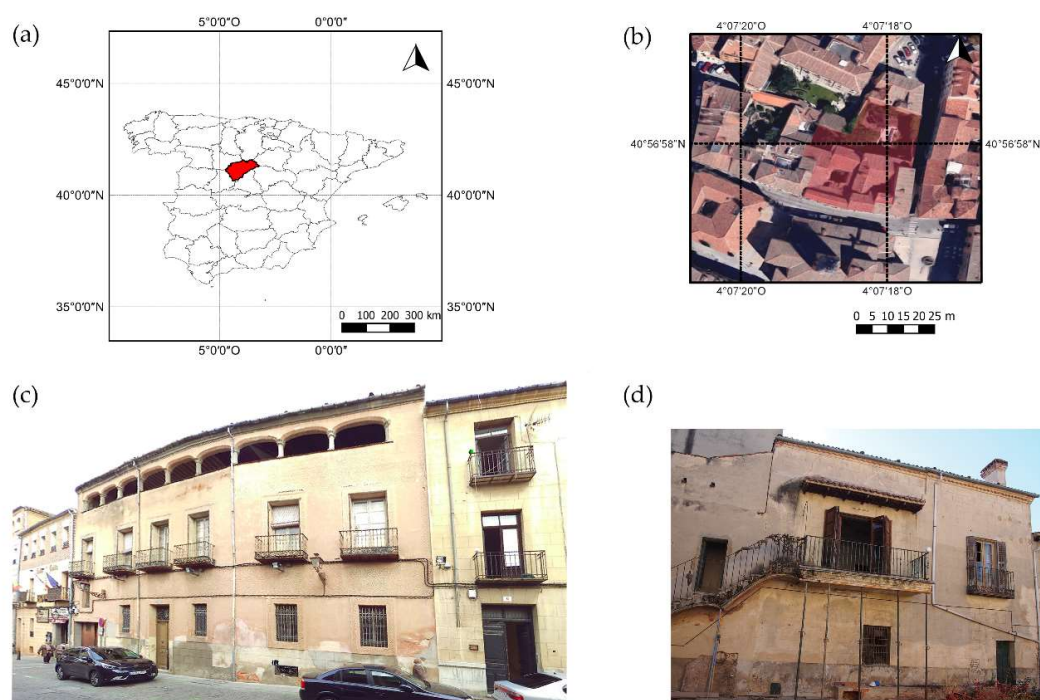
Figure 4. (**a**) Location of the province of Segovia; (**b**) the palace in Segovia; (**c**) main front facade of the palace; (**d**) back front facade of the palace.

Figure 5. Details of the internal cloister.

Timber slabs and open-node (Figure 6) trusses complement these masonry elements. The wooden floors are present both in the simple form, with single beams, and in the form composed of double row of beams and overlapping joists (Figure 7). The secondary frame is made up of a wooden plank in which a conglomerate jet has been made; it is composed of fine aggregates and mortar with a watering function and a thickness of a few centimeters. The finish provides the substrate and the relative flooring.

Figure 6. Gallery; detail of an open-node truss.

Figure 7. Internal cloister; detail of a wooden floor with a double row of beams and overlapping joists.

Nowadays, the state of conservation of the structure is deficient. The infiltration of water and the acid attack promoted by bird excrement have produced the rotting of the wooden elements with the consequent collapse of some floors (Figure 8). Rainfall has also caused the deterioration of sandstone masonry and the detachment of plasters in many environments. The capillary rising of moisture from the foundations has favored saline efflorescence and the appearance of mildew, phenomena accentuated by rainwater. These factors, along with the dust accumulated in the palace's many rooms, make the use of traditional digitalization techniques such as terrestrial photogrammetry or terrestrial laser scanning nearly impossible. These characteristics place the WMLS as the most suitable recording tool due to its flexibility, low weight, and capacity of recording large indoor areas without the support of any position global navigational satellite system (GNSS) [40].

Figure 8. Main cloister; detail of a collapsed wooden floor due to the rotting of the beams.

3.2. Mission Planning

Based on the guidelines previously defined (Sections 2.2.1 and 2.2.2), the surveyed palace was divided into four acquisition paths, each one with a different casuistic found during the digitalization of the heritage buildings (Figure 9):

- path 1 includes interior rooms, the main cloister, and a minimal part of the garden;
- path 2 includes interior rooms, the main cloister, and a part of the garden and a linear gallery;
- path 3 includes interior rooms, the main cloister, and the garden and the street front;
- path 4 includes interior rooms, the main cloister, and a smaller courtyard and the entire garden.

With these premises, the digitization of the internal areas took about 65 min (Table 2). Furthermore, using a terrestrial laser scanner (Faro Focus 3D) with the resolution at 1/5 and the quality at 3x, every scan of the interior took about two and a half minutes. Considering the time needed for the setup of the different stations, a total of 350 min was required for a survey of 70 stations (number compatible with the dimensions of the building), which was six times the period required with the WMLS.

Table 2. General information about the WMLS paths.

Path	Covered Floors	Walked Distance (m)	Acquisition Time (min)	Average Speed (m/s)
1	1	339.80	18.39	0.31
2	4	328.35	17.11	0.32
3	3	426.89	18.47	0.39
4	1	226.70	9.94	0.38

Figure 9. Plan view of the case study.

3.3. Data Processing and Registration

The GeoSLAM algorithm introduced in Section 2.2.3 was controlled by three fundamental parameters:

- The "convergence threshold," which increased or decreased the number of iterations for each processing step during the local and global registration phases. For the case study, a low value of the parameter was chosen, guarantying a quality of data that did not require a large number of iterations;
- the "window size," which defined the size of data samples processed by the algorithm. This helped to encompass the errors that occurred during the local registration phase. An intermediate value for this parameter was a perfect compromise between model quality and required hardware resources;
- the option "prioritize planar surfaces" was used for the case study and considered with very planar surfaces during the global registration phase. This helped to improve the global registration of very large data sets, common in the case of indoor mapping.

This setting guaranteed a processing time of the single path similar to the time required for the detection of the same (Table 3).

Table 3. Processing time of raw data with default setting of full SLAM parameters.

Default Algorithm Configuration		
Path	Processing Time (min)	Difference between Processing and Acquisition time (%)
1	23.18	$\cong$20
2	23.76	$\cong$21
3	25.31	$\cong$25
4	12.42	$\cong$22

It took approximately 83 min (about five times less time that was required to record the seventy stations needed by the terrestrial laser scanner) to solve the full SLAM problem in the four routes.

In order to perform the alignments between the different paths, a network of artificial targets (spheres) wa distributed around the cloister and on the internal and external facades (Figure 10)

(Figure 11). The use of spheres was not mandatory for the execution of the alignment, but this approach made it possible to analyze the registration error between the different paths. The centroids of homologous spheres, extracted by means of the RANSAC Shape Detector algorithm [41] were used as reference pairs. The error associated with the pairs was quantified through the discrepancy in the overall coordinate system between the spatial coordinates of the two homologous centroids (located in two different paths). The root mean square error (RMSE) of the whole registration was just over 3 cm for all the alignment processes achieved (a value perfectly compatible with the WMLS accuracy).
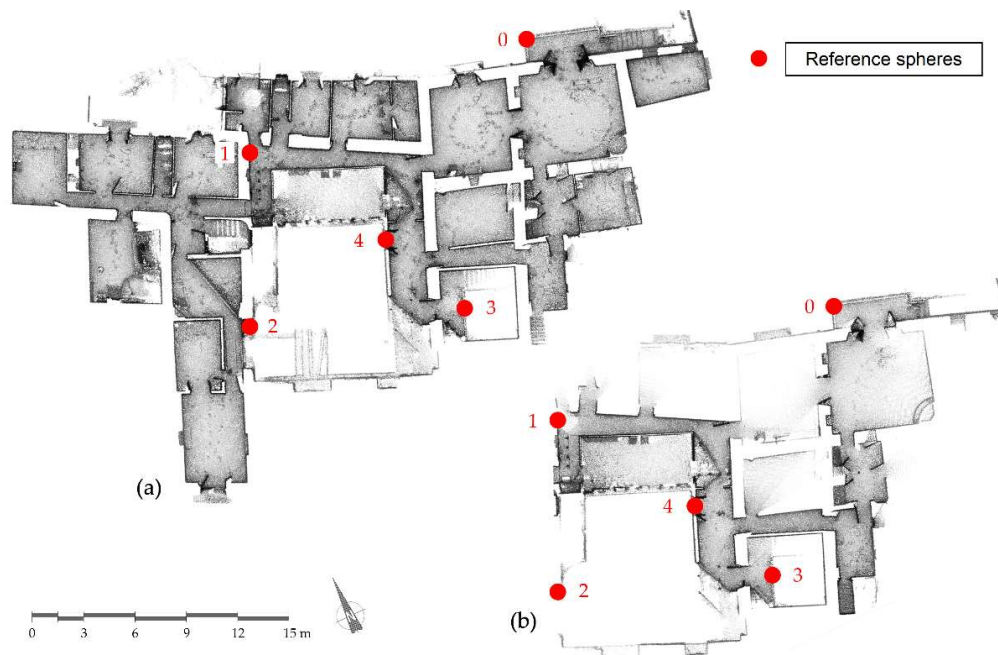
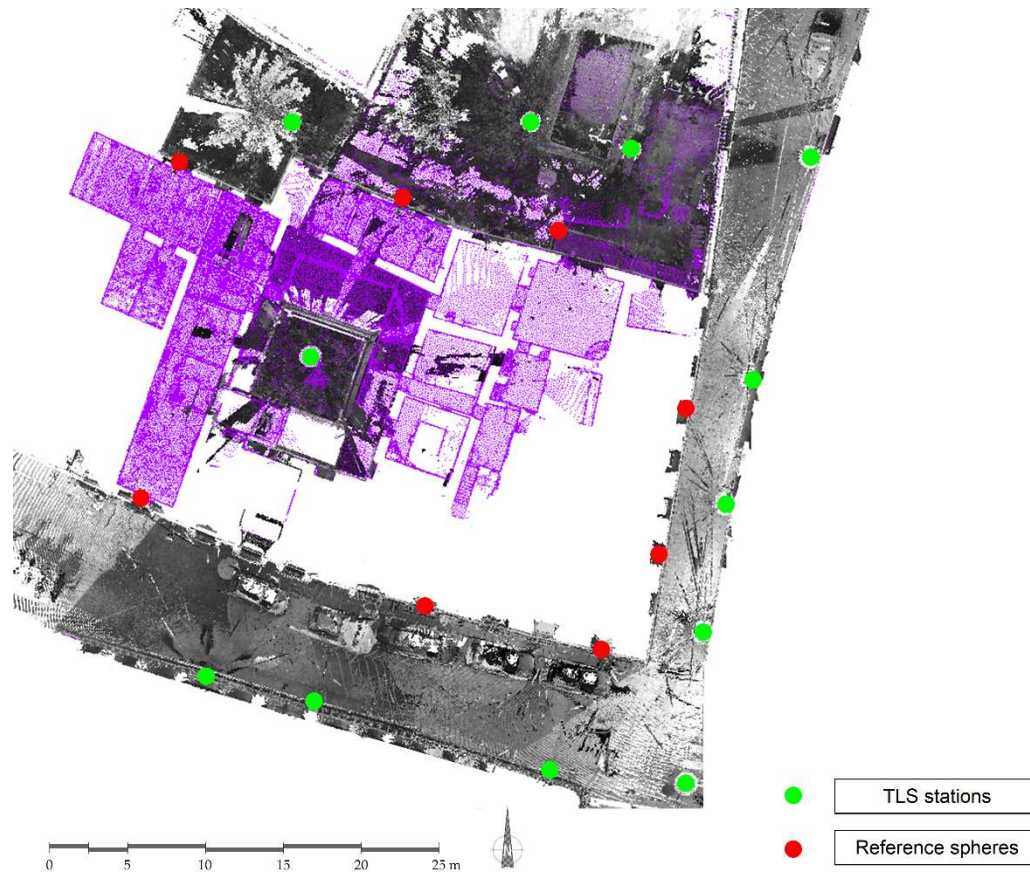**Figure 10.** Reference sphere distribution on the first floor for the path 1 (**a**) and path 2 (**b**).

Figure 11. Reference sphere distribution on the ground floor for the path 3 (**a**) and path 4 (**b**).

3.4. System Validation

A further quality control of the acquired data was performed through a comparison with an outdoor network surveyed with a terrestrial laser scanner (Faro Focus 3D, employed for the detection of the front facade, the garden, and the internal cloister). The network consisted of 11 stations acquired with a resolution of 1/2 and a quality of 2x (Figure 12). The scans were aligned using the spherical targets and then an ICP algorithm, in order to create a ground truth.

Figure 12. Reference sphere distribution on the first floor for the path 2 (red circles) and the outdoor TLS network (green circles). Scans coming from the terrestrial laser scanner are outlined in the grey color, whereas scans coming from the WMLS for the path 2 are represented in the purple color.

Considering the implemented cartographic products, the following validations were carried out: (i) a local validation and (ii) a global validation. The local validation was a comparison based on fitting flat geometric primitives on homologous point clouds. Some distance measurements were extracted, where each value was the mean of five distance measurements between two planes located on the opposite walls or between the floor and ceiling (Figure 13) (Figure 14). Starting from this data, the system was validated trough the indexes introduced by Nocerino et al. [22] (1) (2):

$$\text{RLME} = \left(\frac{D_{Zm} - D_{Fm}}{D_{Fm}} \right) \times 100 \tag{1}$$

$$\text{RLMA} = 1 : \text{ROUND}\left(\left| \frac{100}{\text{RLME}} \right| \right) = 1 : \text{ROUND}\left(\left| \frac{D_{Fm}}{D_{Zm} - D_{Fm}} \right| \right) \tag{2}$$

The relative measurement error (RLME) was computed as the relative difference between measured distance D_Z for the GeoSLAM ZEB-REVO and the distance for the Faro Focus 3D, assumed

as reference length D_F. The relative length measurement accuracy (RLMA) was defined as the rounded absolute reciprocal value of the RLME times 100. Table 4 reports the results.
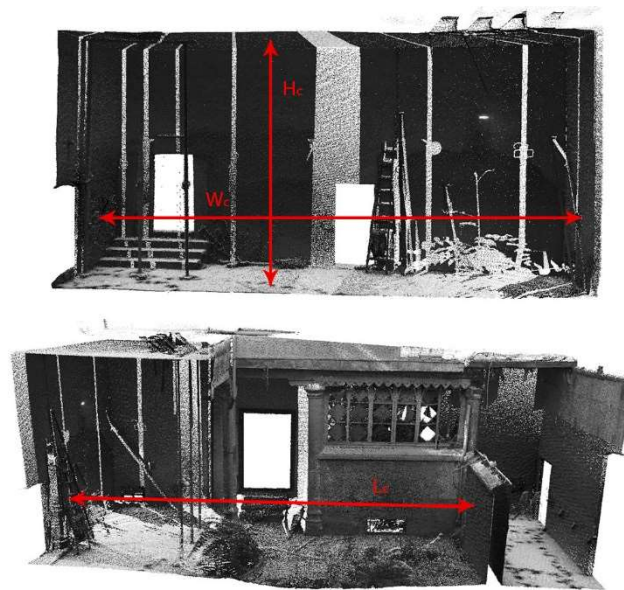

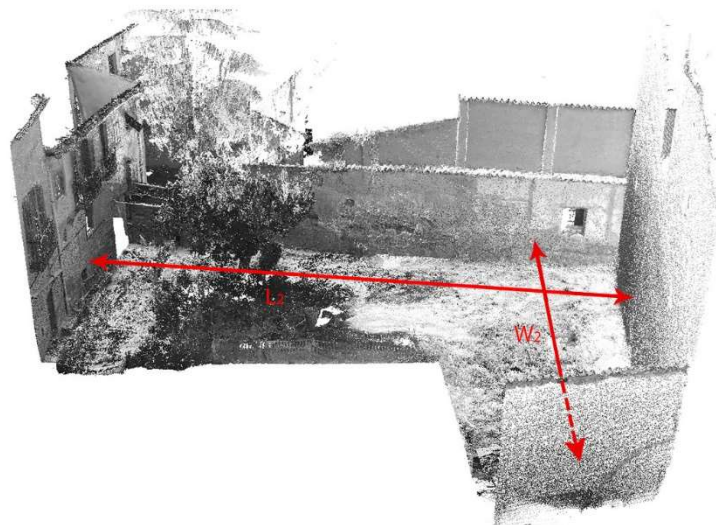**Figure 13.** Distances measured for the accuracy evaluation.

Figure 14. Distances measured for the accuracy evaluation.

Table 4. Measured distances with standard deviations (σ), relative length measurement errors (RMLE) and accuracies (RMLA).

		Faro Focus 3D		GeoSLAM ZEB-REVO			
		D_{Fm} (m)	σ (m)	D_{Zm} (m)	σ (m)	RLME	RLMA
Main cloister	L_1	10.279	0.008	10.268	0.010	−0.107	≈1:1000
	W_1	10.096	0.013	10.085	0.022	−0.109	≈1:600
	H_1	4.869	0.014	4.869	0.012	0.001	≈1:7000
Garden	L_2	22.730	0.012	22.756	0.011	0.114	≈1:800
	W_2	18.766	0.023	18.787	0.025	0.112	≈1:900

In the case of the main garden, the RLME assumed a slightly greater value than the main cloister. This was due to two factors: in the case of a SLAM system, the greater probability of error accumulation over longer distances (L_2 and W_2) and the decline in performance of the latter with outdoor acquisitions (being designed for indoor surveys). The global validation was carried out by comparing the centroids of the sphere network captured by both systems (Figure 12), with an approach similar to the one defined in Section 3.3. The RMSE obtained was around 3 cm, which was in line with the accuracy of the proposed method. In both the validation approaches, the accuracy of the WMLS was between 1 and 3 cm, which was compatible with the data provided by the manufacturer [34].

3.5. Plan and Section Restitution

The post-processing returns 3D point clouds, characterized by the number of points (and therefore of bytes required for its archiving), was not suited for the vectorization of two-dimensional products. Moreover, their density was not uniform, since it was related to the traveling speed along the paths and the overlapping of some parts of the clouds in the registration phase. Table 5 provides a schematic summary of the magnitude and mean surface density values for each point cloud. As can be seen from the comparison with Table 2, an increase in average speed corresponded to a decrease in the mean surface density.

Table 5. Point cloud features; the surface density is estimated by counting for each point the number of neighbors inside a sphere of three centimeters radius (R) and dividing this value by the sphere max section (πR^2).

Path	Number of Points	Mean Surface Density (points/m^2)	Number of Points after 1 cm Subsampling	Mean Surface Density after 1 cm Subsampling (points/m^2)
1	32,955,139	29,648	14,056,546	6140
2	30,059,713	28,399	14,032,348	5594
3	33,839,213	20,428	16,766,690	5348
4	16,720,282	18,488	9,210,536	4634

In order to generate plans and sections, a subsampling strategy based on distance (1 cm) was applied without producing any loss of detail that would compromise the quality of the products. As a result, a 3D point cloud with more than a 100 million points was obtained for the whole historical palace (Figure 15).

The final step involved tracing the two-dimensional products. To do this, several sections along the different floors of the building were extracted. Previously, in the application of the least-cost-path algorithm, a low pass filter was applied [42]. This strategy locally fit a plane around each point of the cloud and then removed those points far from the fitted plane (Figure 16a). For the present case study, the following parameters were used: (i) a neighbored search radius of 0.03 m and (ii) a relative error of 1 sigma for the exclusion of the points. Next, we applied the filtered point cloud using the least-cost-path algorithm, which allowed for the automatic vectorization of the plant (Figure 16b). Finally, some manual adjustments were conducted on the obtained vectorization data, allowing for the creation of plans in a quick and accurate way (Figure 17).
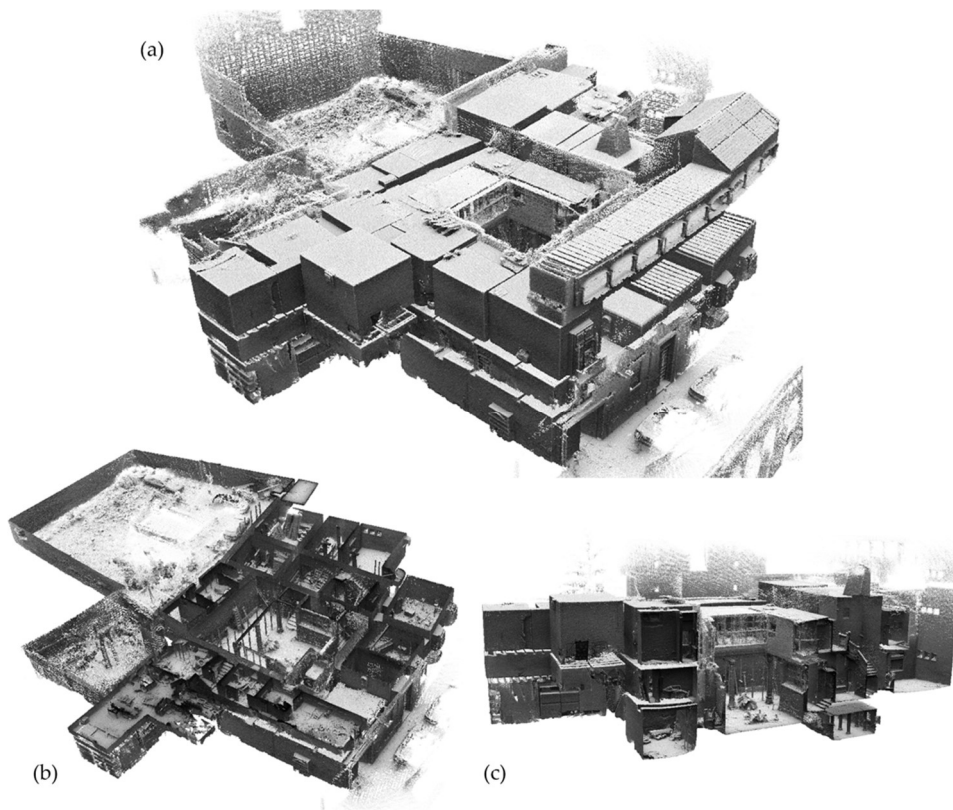
Figure 15. Final point cloud with more than a 100 million points: (**a**) perspective view; (**b**) horizontal section; (**c**) vertical section.
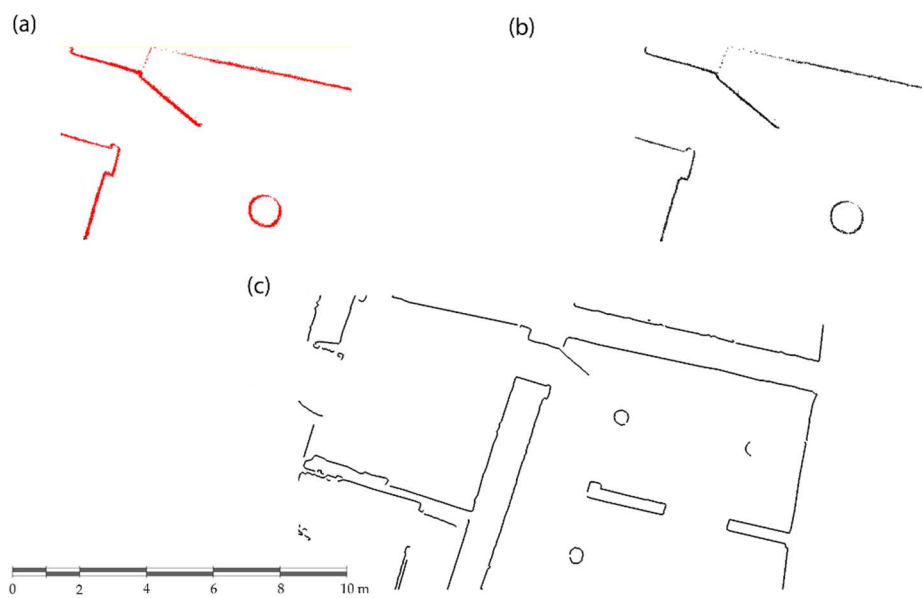
Figure 16. Detail of the vectorization process: (**a**) section extracted from the point cloud; (**b**) section filtered; (**c**) application of the least-cost-algorithm over the filtered section.

Figure 17. Ground floor plan and first floor plan.

4. Discussion

Based on the obtained results, as well as its proven its efficiency, accuracy, portability, and weight, it can be seen that the WMLS tested in our case study offers a potential solution for mapping complex cultural heritage sites.

Regarding the efficiency, the WMLS needed just 63 min to capture the data (distributed in a total of four paths) and 83 min to solve the SLAM problem. In both cases, the system outperformed the time estimated for a terrestrial laser scanner to digitalize the same construction (around 70 scan stations). In comparison with other state-of-the-art MMS, such as the Leica Pegasus back-pack or the Heron MS-2 back-pack, the proposed WMLS solution had a lower data acquisition rate (43,000 points per second against 600,000 points per second captured by the Leica Pegasus back-pack and 700,000 points per second captured by the Heron system). The WMLS capture rate is suitable in terms of its density, capacity to detect geometrical features, and for its ability to map indoor cultural heritage environments.

Regarding the accuracy, the point cloud returned by the WMLS guaranteed an accuracy within a centimeter in relation to the point cloud obtained by a terrestrial laser scanner. These values were similar to those obtained by Nocerino et al. [22] for indoor environments and those obtained by Cabo et al. [43] in an outdoor environment with many geometrical features. This accuracy seems to be linked with the number of geometrical features present in the scene, as well as the planning of the data acquisition using several close-loops.

Concerning the portability, the tested sensor had approximately 4 kg of weight and small dimensions (220 × 180 × 470 mm) (Table 1) in comparison with other MMS, such as the Leica Pegasus backpack, with an estimated weight of 12 kg and dimensions of 310 mm × 270 mm × 730 mm, the Heron MS-2 back-pack mapping solution, with a total weight of 11 kg, and the NavVIS 3D system, which requires a cart to support its sensors [22,24,44]. These characteristics are especially relevant for the digitalization of the palace, since this building shows narrow areas (Figure 8) in which the other MMS would have problems.

5. Conclusions

In this paper, a wearable mobile laser system (WMLS) has been presented and tested for the digitalization of a complex cultural heritage building. This device highlights for its lightweight,

flexibility in comparison with other traditional techniques, such as terrestrial photogrammetry or terrestrial laser scanning. The combination of this instrument, mainly composed by a 2D Hokuyo laser scanner and an Inertial Measurement Unit, together with the Simultaneous Location and Mapping approach, allows the acquisition of indoor environments dynamically without the necessity of stations or the use of global navigation satellite systems.

Investigation results estimate that the WMLS requires the complete digitalization of the entire structure, with around 3000 m^2, in about 65 min. A quick comparison demonstrates how the acquisition time of the wearable system is approximately equal to the sixth part of the time required by the terrestrial laser scanner (Faro Focus 3D), providing the correct accuracy and density of data for the creation of sections and plans for restoration projects. The post-processing phase itself is around five times shorter than the corresponding registration of the laser scans.

The process of registering the different paths, which uses spherical target centroids as control points, returns a RMSE of about 3 cm, compatible with the accuracy of the analyzed system, and is able to offer excellent results in complex environments, such as the one described in this paper. These potentialities are also confirmed by the comparison with an external network generated by a terrestrial laser scanner. During this stage, the accuracy of the system has been evaluated at two different scales: (i) at the local scale using the relative length measurement error (RLME) and the relative length measurement accuracy (RLMA), and (ii) at the global scale, where the root mean square error (RMSE) between the centroids detected by each system, WMLS and laser scanner, have been confronted. In both cases the accuracy of the system is estimated between 1 and 3 cm.

Future investigations could concern the integration of the point clouds generated by the WMLS into building information modelling (BIM) systems. Another future development could concern the process of coloring automatically the point cloud of WMLS by synchronizing the acquisition path with video captured by GoPro and the subsequent projection of the frames on the cloud itself.

Author Contributions: All authors conceived and designed the experimental campaign; A.d.F., L.J.S.-A., and D.G.A. performed the experimental campaign; A.d.F., L.J.S.-A., J.A.M.-J., and R.M. performed the pre-processing and post-processing steps; A.d.F., L.J.S.-A., and S.B. wrote the article and all authors read and approved the final version.

Conflicts of Interest: the authors declare no conflict of interest.

References

1.　Krakow Charter 2000: Principles for Conservation and Restoration of Built Heritage. Available online: http://hdl.handle.net/1854/LU-128776 (accessed on 20 September 2018).

2.　Torres-Martínez, J.A.; Seddaiu, M.; Rodríguez-Gonzálvez, P.; Hernández-López, D.; González-Aguilera, D. A multi-data source and multi-sensor approach for the 3D reconstruction and web visualization of a complex archaelogical site: The case study of "Tolmo De Minateda". *Remote Sens.* **2016**, *8*, 550. [CrossRef]

3.　Garcia-Gago, J.; Gomez-Lahoz, J.; Rodríguez-Méndez, J.; González-Aguilera, D. Historical single image-based modeling: The case of Gobierna Tower, Zamora (Spain). *Remote Sens.* **2014**, *6*, 1085–1101. [CrossRef]

4.　Waldhäusl, P.; Ogleby, C. 3 × 3 rules for simple photogrammetric documentation of architecture. In *International Archives of Photogrammetry and Remote Sensing, Proceedings of the Close Range Techniques and Machine Vision, Melbourne, Australia, 1–4 March 1994*; Australian Photogrammetric and Remote Sensing Society: Melbourne, VIC, Australia, 1994.

5.　Barber, D.; Mills, J. *3D Laser Scanning for Heritage: Advice and Guidance to Users on Laser Scanning in Archaeology and Architecture*; Historic England: Swindon, UK, 2007, ISBN 978-1848025219.

6.　Kraus, K.; Waldhäusl, P. *Photogrammetry: Fundamentals and Standard Processes*; Dümmler Köln: Munich, Germany, 1993, ISBN 978-3427786849.

7.   Fabio, R.; Sabry, E.H. Image-based 3D Modelling: A Review. *Photogramm. Rec.* **2006**, *21*, 269–291. [CrossRef]

8.   Blais, F. Review of 20 years of range sensor development. *J. Electron. Imaging* **2004**, *1*, 13. [CrossRef]

9.   Guidi, G.; Russo, M.; Beraldin, J.-A. *Acquisizione 3D e Modellazione Poligonale*; McGraw-Hill: New York, NY, USA, 2010, ISBN 978-8838665318.

10.   Kalay, Y.; Kvan, T.; Affleck, J. *New Heritage: New Media and Cultural Heritage*, 1st ed.; Routledge: London, UK, 2007, ISBN 978-0415773560.

11.   Torres-Martínez, J.A.; Sánchez-Aparicio, L.J.; Hernández-López, D.; González-Aguilera, D. Combining geometrical and radiometrical features in the evaluation of rock art paintings. *Digital Appl. Archaeol. Cult. Herit.* **2017**, *5*, 10–20. [CrossRef]

12.   Gonzalez-Aguilera, D.; Muñoz-Nieto, A.; Rodriguez-Gonzalvez, P.; Menéndez, M. New tools for rock art modelling: Automated sensor integration in Pindal Cave. *J. Archaeol. Sci.* **2011**, *38*, 120–128. [CrossRef]

13.   Sánchez-Aparicio, L.J.; Riveiro, B.; Gonzalez-Aguilera, D.; Ramos, L.F. The combination of geomatic approaches and operational modal analysis to improve calibration of finite element models: A case of study in Saint Torcato Church (Guimarães, Portugal). *Constr. Build. Mater.* **2014**, *70*, 118–129. [CrossRef]

14.   Sánchez-Aparicio, L.J.; Del Pozo, S.; Ramos, L.F.; Arce, A.; Fernandes, F.M. Heritage site preservation with combined radiometric and geometric analysis of TLS data. *Autom. Constr.* **2018**, *85*, 24–39. [CrossRef]

15.   Del Pozo, S.; Herrero-Pascual, J.; Felipe-García, B.; Hernández-López, D.; Rodríguez-Gonzálvez, P.; González-Aguilera, D. Multispectral radiometric analysis of façades to detect pathologies from active and passive remote sensing. *Remote Sens.* **2016**, *8*, 80. [CrossRef]

16.   Guidi, G.; Beraldin, J.-A.; Ciofi, S.; Atzeni, C. Fusion of range camera and photogrammetry: A systematic procedure for improving 3-D models metric accuracy. *IEEE Trans. Syst. Man Cybern. B* **2003**, *33*, 667–676. [CrossRef] [PubMed]

17.   Stumpfel, J.; Tchou, C.; Yun, N.; Martinez, P.; Hawkins, T.; Jones, A.; Emerson, B.; Debevec, P.E. Digital Reunification of the Parthenon and its Sculptures. In Proceedings of the VAST, Brighton, UK, 5–7 November 2003; pp. 41–50.

18.   Paparoditis, N.; Papelard, J.-P.; Cannelle, B.; Devaux, A.; Soheilian, B.; David, N.; Houzay, E. Stereopolis II: A multi-purpose and multi-sensor 3D mobile mapping system for street visualisation and 3D metrology. *Rev. Fr. Photogramm. Teledetec.* **2012**, *200*, 69–79.

19.   Remondino, F.; Toschi, I.; Orlandini, S. Mobyle Mapping Systems: Recenti sviluppi e caso applicativo. *GEOmedia* **2015**, *19*, 6–10.

20.   Al-Hamad, A.; El-Sheimy, N. Smartphones based mobile mapping systems. *Int. Arch. Photogramm. Remote Sens. Spat. Inf. Sci.* **2014**, *40*, 29. [CrossRef]

21.   Piras, M.; Di Pietra, V.; Visintini, D. 3D modeling of industrial heritage building using COTSs system: Test, limits and performances. *Int. Arch. Photogramm. Remote Sens. Spat. Inf. Sci.* **2017**, *42*, 281. [CrossRef]

22.   Nocerino, E.; Menna, F.; Remondino, F.; Toschi, I.; Rodríguez-Gonzálvez, P. Investigation of indoor and outdoor performance of two portable mobile mapping systems. In *Videometrics, Range Imaging, and Applications XIV*; International Society for Optics and Photonics: Munich, Germany, 2017.

23.   Kumar, G.A.; Patil, A.K.; Patil, R.; Park, S.S.; Chai, Y.H. A lidar and imu integrated indoor navigation system for uavs and its application in real-time pipeline classification. *Sensors* **2017**, *17*, 1268. [CrossRef] [PubMed]

24.   Lehtola, V.V.; Kaartinen, H.; Nüchter, A.; Kaijaluoto, R.; Kukko, A.; Litkey, P.; Honkavaara, E.; Rosnell, T.; Vaaja, M.T.; Virtanen, J.-P. Comparison of the selected state-of-the-art 3d indoor scanning and point cloud generation methods. *Remote Sens.* **2017**, *9*, 796. [CrossRef]

25.   Flener, C.; Vaaja, M.; Jaakkola, A.; Krooks, A.; Kaartinen, H.; Kukko, A.; Kasvi, E.; Hyyppä, H.; Hyyppä, J.; Alho, P. Seamless mapping of river channels at high resolution using mobile lidar and uav-photography. *Remote Sens.* **2013**, *5*, 6382–6407. [CrossRef]

26.   Opromolla, R.; Fasano, G.; Rufino, G.; Grassi, M.; Savvaris, A. LiDAR-inertial integration of UAV localization and mapping in complex enviroments. In Proceedings of the 2016 International Conference on Unmanned Aircraft Systems (ICUAS), Arlington, VA, USA, 7–10 June 2016.

27.   Niu, X.; Yu, T.; Tang, J.; Chang, L. An online solution of lidar scan matching aided inertial navigation system for indoor mobile mapping. *Mob. Inf. Syst.* **2017**, *2017*, 4802159. [CrossRef]

28.   Shamseldin, T.; Manerikar, A.; Elbhnasawy, M.; Habib, A. SLAM-based Pseudo-GNSS/INS Localization System for Indoor LiDAR Mobile Mapping Systems. In Proceedings of the IEEE/OIN PLANS 2018, Monterey, CA, USA, 23–26 April 2018.

29.   Pierzchała, M.; Giguère, P.; Astrup, R. Mapping forests using an unmanned ground vehicle with 3D LIDAR and graph-SLAM. *Comput. Electron. Agric.* **2018**, *145*, 217–225. [CrossRef]

30.   Lagüela, S.; Dorado, I.; Gesto, M.; Arias, P.; González-Aguilera, D.; Lorenzo, H. Behavior analysis of novel wearable indoor mapping system based on 3d-slam. *Sensors* **2018**, *18*, 766. [CrossRef] [PubMed]

31.   Farella, E. 3d mapping of underground environments with a hand-held laser scanner. In Proceedings of the SIFET Annual Conference, Lecce, Italy, 8–10 June 2016.

32.   Thrun, S. Simultaneous localization and mapping. In *Robotics and Cognitive Approaches to Spatial Mapping*; Jefferies, M.E., Yeap, W., Eds.; Springer: Luxembourg, 2008; pp. 13–41, ISBN 978-3-540-75388-9.

33.   Bosse, M.; Zlot, R.; Flick, P. Zebedee: Design of a spring-mounted 3-d range sensor with application to mobile mapping. *IEEE Trans. Robot.* **2012**, *28*, 1104–1119. [CrossRef]

34.   GeoSLAM Technology, ZEB-REVO Solution Brochure. Available online: https://gpserv.com/wp-content/uploads/2017/01/ZEB-REVO-Brochure-v1.0.3.pdf (accessed on 15 August 2018).

35.   Quigley, M.; Conley, K.; Gerkey, B.; Faust, J.; Foote, T.; Leibs, J.; Wheeler, R.; Ng, A.Y. ROS: An open-source Robot Operating System. In Proceedings of the ICRA Workshop on Open Source Software, Kobe, Japan, 12–17 May 2009; p. 5.

36.   Kavanagh, B.F. *Surveying Principles and Applications*, 7th ed.; Pearson Education: Upper Saddle River, NJ, USA, 2006, ISBN 978-0137009404.

37.   Grisetti, G.; Kummerle, R.; Stachniss, C.; Burgard, W. A tutorial on graph-based SLAM. *IEEE Intell. Transp. Syst. Mag.* **2010**, *2*, 31–43. [CrossRef]

38.   Thiele, S.T.; Grose, L.; Samsu, A.; Micklethwaite, S.; Vollgger, S.A.; Cruden, A.R. Rapid, semi-automatic fracture and contact mapping for point clouds, images and geophysical data. *Solid Earth* **2017**, *8*, 1241. [CrossRef]

39.   Navarro, P.C. The Royal Country Estates around the Monastery of El Escorial: Medieval Tradition and Flemish Influence. *Rev. EGA* **2014**, 46–53. [CrossRef]

40.   Misra, P.; Enge, P. *Global Positioning System: Signals, Measurements and Performance*, 2nd ed.; Ganga-Jamuna Press: Lincoln, MA, USA, 2010, ISBN 9780970954428.

41.   Schnabel, R.; Wahl, R.; Klein, R. Efficient RANSAC for point-cloud shape detection. In *Computer Graphics Forum*; Blackwell Publishing Ltd.: Oxford, UK, 2007; pp. 214–226.

42.   Han, X.-F.; Jin, J.S.; Wang, M.-J.; Jiang, W.; Gao, L.; Xiao, L. A review of algorithms for filtering the 3D point cloud. *Signal Process. Image Commun.* **2017**, *57*, 103–112. [CrossRef]

43.   Cabo, C.; Del Pozo, S.; Rodríguez-Gonzálvez, P.; Ordóñez, C.; González-Aguilera, D. Comparing Terrestrial Laser Scanning (TLS) and Wearable Laser Scanning (WLS) for individual Tree Modeling at Plot Level. *Remote Sens.* **2018**, *10*, 540. [CrossRef]

44.   Heron Wearable Mobile Mapping. Available online: https://gexcel.it/en/solutions/heron-mobile-mapping (accessed on 18 November 2018).